TsetlinKWS: A 65nm 16.58µW, 0.63mm² State-Driven Convolutional Tsetlin Machine-Based Accelerator For Keyword Spotting

Baizhou Lin*, Yuetong Fang*, Renjing Xu, Rishad Shafik, Senior Member, IEEE, Jagmohan Chauhan

Abstract—The Tsetlin Machine (TM) has recently attracted attention as a low-power alternative to neural networks due to its simple and interpretable inference mechanisms. However, its performance on speech-related tasks remains limited. This paper proposes TsetlinKWS, the first algorithm-hardware codesign framework for the Convolutional Tsetlin Machine (CTM) on the 12-keyword spotting task. Firstly, we introduce a novel Mel-Frequency Spectral Coefficient and Spectral Flux (MFSC-SF) feature extraction scheme together with spectral convolution, enabling the CTM to reach its first-ever competitive accuracy of 87.35% on the 12-keyword spotting task. Secondly, we develop an Optimized Grouped Block-Compressed Sparse Row (OG-BCSR) algorithm that achieves a remarkable 9.84× reduction in model size, significantly improving the storage efficiency on CTMs. Finally, we propose a state-driven architecture tailored for the CTM, which simultaneously exploits data reuse and sparsity to achieve high energy efficiency. The full system is evaluated in 65 nm process technology, consuming 16.58 µW at 0.7 V with a compact 0.63 mm² core area. TsetlinKWS requires only 907k logic operations per inference, representing a $10 \times$ reduction compared to the state-of-the-art KWS accelerators, positioning the CTM as a highly-efficient candidate for ultra-low-power speech applications.

Index Terms—Tsetlin Machine (TM), keyword spotting (KWS), machine learning accelerator, speech feature extraction, model compression.

I. INTRODUCTION

THE Tsetlin Machine (TM) is an emerging machine learning algorithm founded on propositional logic and learning automata. It operates on binary inputs and performs logical pattern matching for inference. Different from neural networks (NNs), its logic-based and multiplication-free computational paradigm offers greater suitability for low-power edge deployment. Furthermore, its straightforward state update strategy without backpropagation makes it well-suited for ondevice learning. These characteristics of the TM are essential for edge speech applications, e.g., keyword spotting (KWS), which have stringent requirements for low power consumption, low latency, and on-device adaptability.

Existing NN-based KWS accelerators follow either the batch-based or frame-based processing paradigm, as shown in Fig. 1. The frame-based accelerators, represented by recurrent

*These authors contributed equally to this work.

Baizhou Lin is with the University of Southampton, SO17 1BJ Southampton, U.K. (e-mail: bzlin713@163.com).

Yuetong Fang, and Renjing Xu are with The Hong Kong University of Science and Technology (Guangzhou), 511453 Guangzhou, China.

Rishad Shafik is with the Microsystems Research Group, School of Engineering, Newcastle University, NE1 7RU Newcastle upon Tyne, U.K.

Jagmohan Chauhan is with the University College London, WC1E 6BT

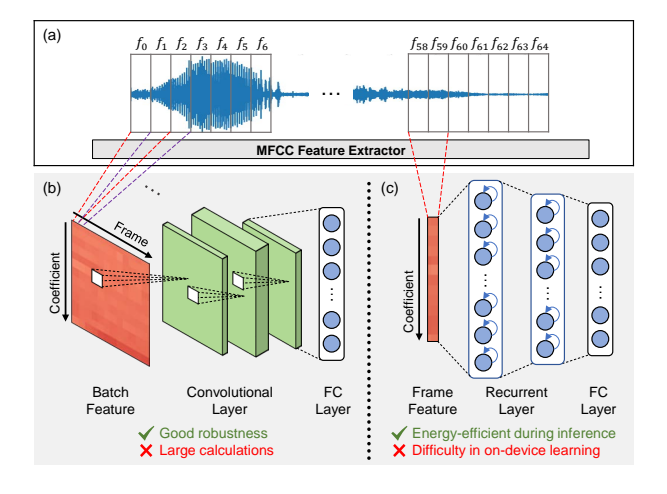


Fig. 1. NN-based KWS accelerator categories. (a) Audio signal. (b) Batch-based accelerators are represented by convolutional neural networks [4], [5], [6], [7]. They perform inference in a multi-frame manner because neurons do not have states. (c) Frame-based accelerators are represented by recurrent neural networks [8], [9], [10], [11]. They process only one frame of features per inference.

neural networks (RNNs), enable energy-efficient inference as they can reuse hidden states across time and reduce redundant computation. However, during the training phase, the intermediate activations and hidden states of the multi-layer RNN need to be expanded in the time dimension and be buffered in the memory. This substantial memory overhead limits the prospect of frame-based accelerators for on-device learning. The simple inference and learning mechanisms of TMs present a new solution for this challenge. Previous studies have shown that TMs achieve competitive accuracy and energy benefits compared with NNs on simple datasets [1], while also exhibiting a clear advantage in on-device learning [2], [3]. However, two current challenges hinder their widespread adoption in edge deployment: firstly, for more complex tasks such as speech recognition, their performance remains limited relative to NN-based methods; secondly, there is still a lack of a hardware architecture tailored for the Convolutional Tsetlin Machine (CTM) to fully leverage its sparsity advantage while maintaining efficient data reuse.

In this work, we focus on the KWS problem to explore the limitations of TMs on speech tasks. KWS is a representative low-power edge application, widely used to enable wake-up and command functions. Its always-on mode and tight energy budgets impose particularly stringent requirements on latency, power consumption, and model efficiency, making it a critical test case for TM-based methods. However, existing

approaches that apply the Vanilla TM to KWS have failed to deliver competitive accuracy. This limitation arises because Vanilla TMs rely on long-term pattern matching over Boolean features, which hampers the model's generalization ability. This tendency is evident in experimental results: Lei et al. [12] observed that increasing the number of target keywords from six to nine led to a considerable accuracy reduction, from 86.5% to 80.5%. Subsequent work reveals a similar issue: although REDRESS introduced compression-aware training to refine Tsetlin Automata (TAs) and attained 87.1% accuracy, this gain was confined to a simplified 6-keyword task [13]. There remains a persistent difficulty of scaling Vanilla TMs to more complex scenarios.

Beyond the algorithmic limitations of TM in speech tasks, a second critical challenge lies in the architectural mismatch between existing accelerators and the computational paradigm of the CTM. Current CTM-based accelerator designs are largely inherited from Convolutional Neural Networks (CNNs) accelerators, which are unable to efficiently achieve both data reuse and sparse utilization due to the constraints of NNs. As a result, the unique highly bit-sparsity and deterministic sparsity of CTMs cannot be fully utilized. Tunheim et al. [14] proposed a CTM image classification accelerator that does not support sparse utilization. The ineffective computation brought by its CNN-style dense architecture leads to the actual irrationality of bandwidth, that is, due to high concurrency requirements, the model can only be stored in registers. To overcome these inefficiencies, we systematically analyze the computational patterns of CTMs and the design principles of existing edge Artificial Intelligence (AI) accelerators, leading us to propose a new architecture that simultaneously enables sparse acceleration and efficient data reuse.

In this paper, we address the challenges of low accuracy and limited hardware efficiency of CTMs on speech tasks by designing a KWS inference-only accelerator. Firstly, for the feature processing, we introduce a Mel-Frequency Spectral Coefficient and Spectral Flux (MFSC-SF) algorithm to enhance feature quality, and a streaming threshold update circuit for efficient feature binarization. Secondly, to address storage constraints, we apply block and grouped compressions, formulated as a maximum weight matching problem, for finding the optimal compressed model size. Thirdly, we propose a state-driven architecture that enables sparse acceleration and efficient data reuse. Finally, we adopt a two-stage simulated annealing algorithm for balanced clause scheduling. The main contributions of this work are summarized as follows:

- Algorithmic Improvement for CTM-based KWS: We introduce a novel MFSC-SF algorithm and spectral convolution operation for CTMs, achieving 87.35% accuracy on a 12-keyword spotting task. This marks the first time a CTM has delivered competitive performance against edge-deployed NNs on this benchmark.
- CTM-Specific Accelerator: We design an efficient state-driven accelerator tailored for CTMs that unlocks high data reuse and full utilization of sparsity, achieving a remarkable power of $16.58~\mu W$ within a compact core area of $0.63~mm^2$.
- Edge-Optimized Deployment: We propose an Opti-

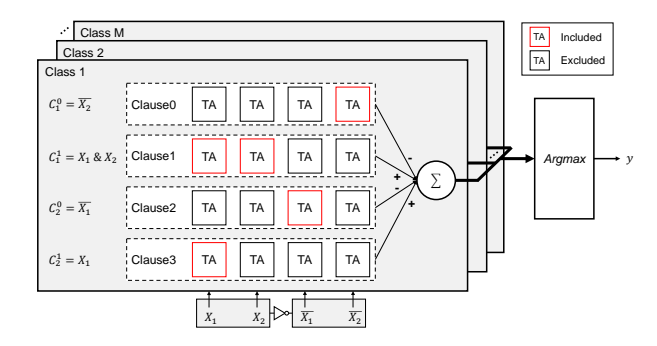


Fig. 2. The structure of the Tsetlin Machine. X_k refers to the Boolean input. Included TAs and excluded TAs determine the matching pattern of clause C_i^j .

mized Grouped Block-Compressed Sparse Row (OG-BCSR) algorithm and a two-stage scheduling scheme, achieving a $9.84 \times$ model size reduction and a 12.2% PE utilization improvement.

The rest of this paper is structured as follows: Section II reviews the background of CTM and its associated hardware/algorithm design challenges; Section III details the proposed state-driven CTM-based KWS system; Section IV presents and analyzes the implementation results; Finally, we summarize our work in Section V.

II. BACKGROUND AND CHALLENGES

A. Compression for Tsetlin Machines

The TM is a logic-based learning algorithm that uses a set of logical clauses to capture discriminative patterns in data. As shown in Fig. 2, the input to a TM is a set of Boolean literals, namely variables and their negations. Each clause consists of multiple TAs operating independently to decide whether a literal should be included or excluded from the clause. Through this collective decision-making, the clause converges to a Boolean expression that captures a specific discriminative pattern in the data. When a Boolean expression is satisfied, the weight associated with the corresponding clause is summarized to the class confidence [15]. Ultimately, after processing all clauses of each class, the argmax unit identifies the class with the highest confidence as the prediction result. Similar to CNNs, CTMs [16] introduce a convolutional mechanism that enables parameter sharing by applying the same clauses across multiple input regions. Specifically, as long as the convolution kernel is aligned with the target pattern in any sliding window, the corresponding clause is satisfied. For trained TMs, a key characteristic is their extreme sparsity, with included TAs accounting for only about 1%, resulting in a highly condensed representation.

This high bit-sparsity presents a critical opportunity for compressing TM models, which is particularly desirable for edge deployment. However, existing methods often apply compression algorithms directly to the model parameters, without introducing special treatments for the extreme sparsity. For example, Bakar et al. [17] utilized run-length encoding (RLE) to achieve a 98.68% compression rate on a 6-keyword spotting task, while Maheshwari et al. [13] proposed include-encoding with compression-aware training to reduce model

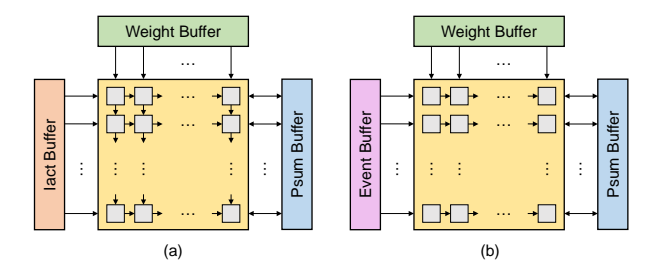


Fig. 3. Two common energy-efficient edge accelerator architectures. (a) Data-driven architecture: efficient for data reuse but inflexible for sparse acceleration. (b) Event-driven architecture: efficient for sparse acceleration but limited in data reuse.

size from 1325.4 KB to 15.4 KB on the same task. We observe that an extremely high sparsity rate, e.g., 99%, can have a counterproductive effect on compression efficiency. To address this issue, we propose block compression and grouped compression schemes to achieve efficient compression, which substantially reduce the average storage overhead per class compared to prior approaches.

B. Architectural Dilemma

Previous CTM accelerators often directly followed NN-based accelerators without a systematic analysis of their underlying design principles, leading to computational inefficiency. Indeed, the properties of the CTM enable us to overcome the limitations of NN-oriented accelerator designs and achieve greater efficiency. In edge AI accelerators, data reuse and sparsity utilization are critical for improving energy efficiency, while simultaneously achieving both goals has remained challenging under NN computing paradigms. As illustrated in Fig. 3, two common architectures exemplify this trade-off.

Data-driven architectures, commonly employing systolic arrays, leverage the regular dataflow of Artificial Neural Networks (ANNs) to maximize data reuse and parallelism [18]. Specifically, weights and input activations (iacts) are propagated simultaneously to realize data reuse. However, sparse ANNs [19] cannot directly benefit from this hardware due to irregular dataflow. Although several works [20], [21], [22] have proposed solutions for efficient sparse utilization, this inherent limitation results in additional hardware overhead, such as expensive index modules and intersection strategies. Therefore, sparse utilization is difficult to achieve efficiently at a low cost in data-driven architectures.

From the perspective of high sparsity, another model more similar to TMs is the Spiking Neural Network (SNN), which has spurred the development of event-driven architecture. This architecture represents a new design paradigm that achieves sparsity acceleration by processing only the data required for spiking events. However, because spiking events are unpredictable and unstructured, weights are difficult to reuse vertically. For instance, SpinalFlow [23] supports only unrolling output channels in a 1×128 Process Element (PE) array due to the inability to reuse weights between spiking events. Some works [24], [25] have constructed event-driven accelerators and compared them with FINN [26]. The results also show

that inefficient data reuse greatly affects the energy efficiency of event-driven accelerators.

We found that the limited benefit of data-driven accelerators supporting sparse acceleration stems from the modest sparsity rate and multi-bit data, while the underwhelming benefit of event-driven accelerators arises from uncertain spiking events. Fortunately, CTMs are highly sparse, logic-based, and sparse-deterministic, which motivates us to propose a state-driven architecture that simultaneously achieves sparse utilization and efficient data reuse, making it particularly suitable for low-power edge applications.

C. Power and Performance Breakdown in KWS

The keyword spotting accelerator typically consists of a front-end feature extractor and a back-end classifier.

To reduce the power consumption of the KWS system, the feature extractor must generate compact yet discriminative representations to reduce the computational burden of the back-end classifier while maintaining accuracy. Related research has shown that binary features are sufficient for KWS tasks. Jiao et al. [27] utilized a Log Mel-Frequency Spectral Coefficient (MFSC) algorithm with fixed thermometer codes to introduce Boolean inputs in the early stage for Binary Neural Networks (BNNs), alleviating computational demands significantly. However, existing binarization methods often rely on fixed thresholds, making them vulnerable to sensor degradation and environmental variations. Additionally, directly using MFSC as the input feature for logic-based models (i.e., TMs) will lead to accuracy loss. To address these issues, we propose an improved feature extraction algorithm with a dynamic binarization method to enhance performance and robustness.

The back-end classifier can be categorized into two types to analyze the power consumption, as illustrated in Fig. 1. Batch-based accelerators process a long-term window of features, incurring higher computational cost (e.g., 3 million operations per inference [6]) for superior noise robustness. In contrast, frame-based accelerators operate in a streaming fashion, processing input frame by frame following the stateful nature of RNNs. This paradigm avoids recomputing features over long windows, representing a more energy-efficient choice for speech tasks. For instance, Chen et al. [10] proposed a delta-encoder module to differentiate input features and generate sparse events to drive RNN model computation, requiring a maximum of only 15 kilo operations per inference.

While TMs are often claimed to be efficient [28], comparisons are frequently made against non-optimized NNs. A more rigorous evaluation, however, requires benchmarking state-of-the-art (SoTA), highly optimized silicon implementations. Our TsetlinKWS accelerator belongs to the batch-based accelerator. In this work, we not only demonstrate the performance of CTMs in speech areas but also aim to showcase their competitive computational power consumption with frame-based accelerators when crossing classification boundaries.

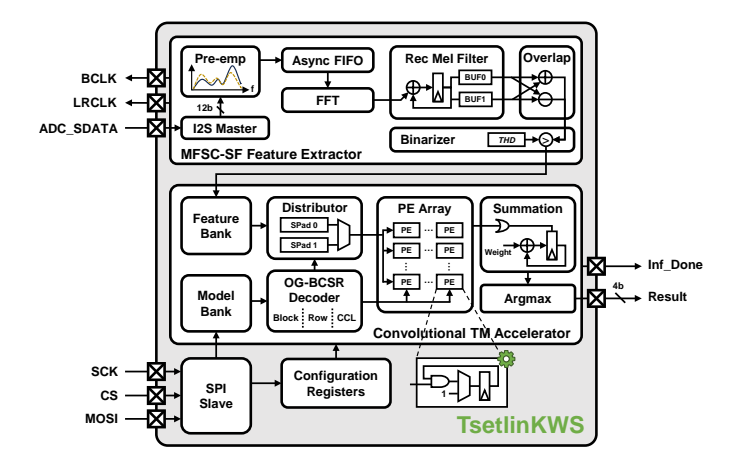


Fig. 4. The system architecture of TsetlinKWS.

III. STATE-DRIVEN CONVOLUTIONAL TSETLIN MACHINE KWS ACCELERATOR

In this section, we elaborate on the end-to-end design of the proposed system. Section III-A outlines the overall architecture of TsetlinKWS. Section III-B details the algorithm and hardware implementation of the MFSC-SF feature extractor. The OG-BCSR compression algorithm is introduced in Section III-C. Finally, Section III-D explains the state-driven strategy.

A. Architecture Overview

Fig. 4 illustrates the system architecture of the proposed TsetlinKWS. TsetlinKWS primarily consists of three components: the Serial Peripheral Interface (SPI) configuration interface, an MFSC-SF feature extractor, and a convolutional TM accelerator. The SPI interface is used for chip configuration and model loading. Audio data is received through the Integrated Interchip Sound (I2S) interface. The feature extractor is used for extracting and binarizing input speech features. The CTM accelerator is constructed to achieve efficient sparse dataflow utilization by algorithm-hardware codesign. Specifically, the OG-BCSR decoder enables horizontal data reuse of feature data through synchronous decompression. The distributor transmits data to the subsequent PE array according to the decompression signal. The PE array is a 58×5 logical array, with each column processing sliding literal data for 58 windows in parallel. When a batch of clauses is completed, 40 clause results are serially transferred to the summation module for confidence updating. Once all clauses for all classes are completed, the argmax module updates the inference result and synchronously sends an interrupt signal to the external. TsetlinKWS is an open-source accelerator available at: https://github.com/Baizhou-713/TsetlinKWS.

B. MFSC-SF Feature Extractor

1) Overview: As illustrated in Fig. 5(a), the conventional Mel-Frequency Cepstral Coefficients (MFCC) extraction pipeline begins with a pre-emphasis filter to compensate for spectral tilt and amplify high-frequency components. The signal is then segmented into overlapped frames and multiplied

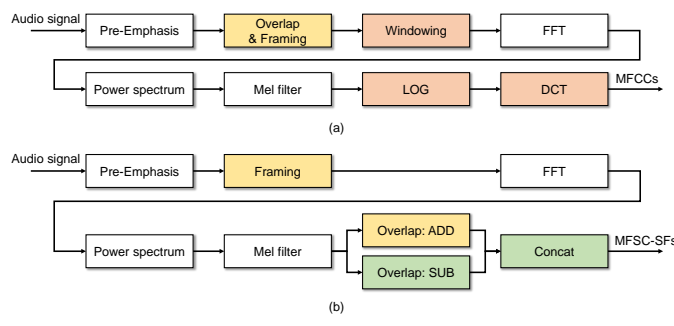


Fig. 5. Feature extraction process: (a) Traditional MFCC flow. (b) The proposed MFSC-SF flow. An additional overlap difference is proposed to achieve the calculation of spectral flux, and some sub-modules are deleted.

by a window function, typically with length N and 50% overlap. An N-point FFT converts each frame to the frequency domain, from which the power spectrum is computed, yielding N/2+1 coefficients. These are passed through a Mel-scale filterbank to produce M Mel-spectral coefficients, where M typically ranges from 26 to 32. Logarithmic compression (LOG) followed by a discrete cosine transform (DCT) is then applied to obtain the MFCC representation.

The proposed MFSC-SF algorithm builds upon the work in [29]. As illustrated in Fig. 5(b), the overlap operation is deferred until after the Mel filterbank, where the effect is achieved by summing the MFSCs of adjacent frames. This modification reduces the subframe length by half, thereby lowering buffer and FFT resource requirements. In addition, several power-saving strategies are adopted: (1) elimination of the windowing operation, (2) approximation of the power spectrum by absolute values, and (3) substitution of triangular Mel filters with rectangular filters. These simplifications incur less than 1% accuracy loss while significantly reducing energy consumption.

To make spectral features easier to extract by CTMs, several additional changes are introduced in the MFSC-SF flow. We remove the LOG and DCT operations for two reasons. First, the single-layer CTM model demonstrates limited ability to learn discriminative features after nonlinear transformations; second, the DCT will convert the feature to a non-local feature, which conflicts with the proposed spectral convolution. Furthermore, distinct from the conventional MFCC flow, we introduce Spectral Flux (SF) to improve accuracy for CTMs. While SF is traditionally defined as the FFT difference between adjacent frames, here it is repositioned after the Mel filter to align with the MFSC. The final feature representation is thus obtained by concatenating the MFSC and SF components.

2) Architectural Design: Fig. 6 illustrates the overall architecture of the proposed feature extractor. The pre-emphasis module follows the design in [6]. Each subframe has a fixed length of 256 samples and is buffered using an asynchronous first-in-first-out (FIFO) buffer, with the frame clock serving as the write clock and the system clock as the read clock. A 256-point FFT is implemented using an eight-stage radix-2 single-path delay feedback (R2-SDF) architecture. To reduce power and storage overhead, stage-wise quantization is ap-

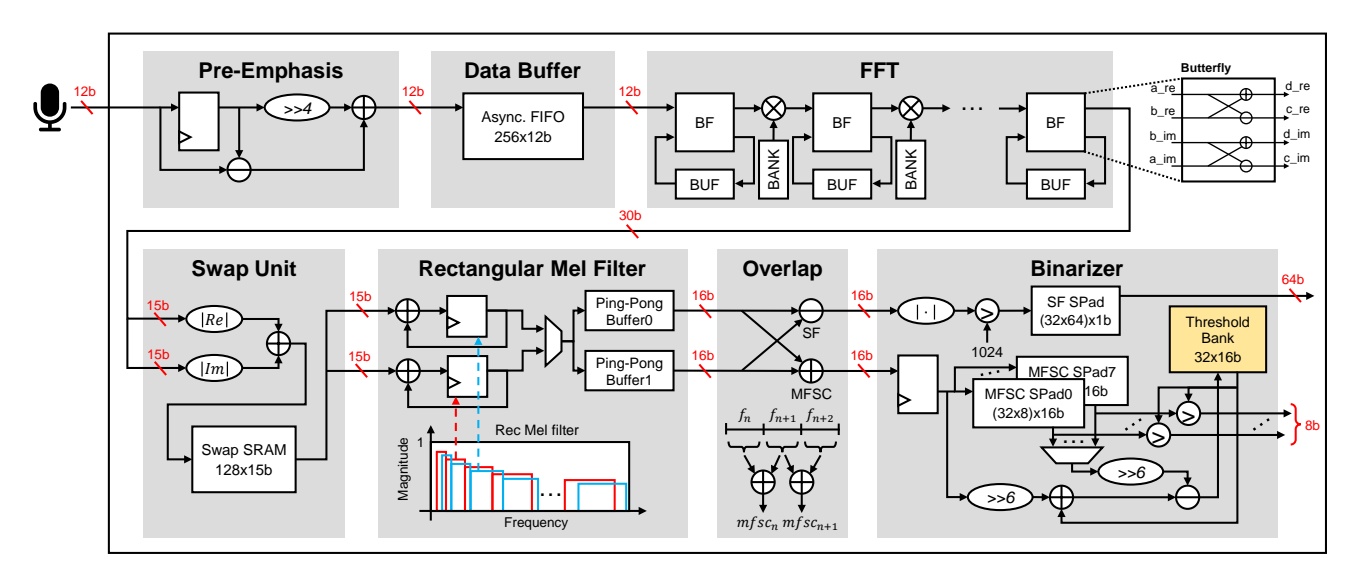


Fig. 6. The architecture diagram of the MFSC-SF feature extractor. MFSC and SF are obtained in the overlap unit and then are binarized in the binarizer. MFSC is binarized using the dynamic mean, while SF is binarized using a fixed threshold.

plied: the integer bit widths are [12, 13, 13, 13, 14, 14, 14, 15], while the fractional bit widths are [1, 1, 1, 1, 1, 0, 0, 0], resulting in a 15-bit FFT output. For a 256-point real FFT, 129 spectral coefficients are retained; one coefficient is discarded for hardware simplification without accuracy degradation. The Mel filter unit employs two registers to compute odd and even filter outputs separately. By adopting rectangular filters with unity gain, multiplication operations are entirely eliminated. A ping-pong buffer stores the results of adjacent frames, enabling overlap processing. SF is then computed in the overlap unit using only a subtractor, yet it provides substantial accuracy improvements. Finally, a binarizer converts the 16-bit outputs into compact binary feature representations.

In this work, we design a binarization circuit for the CTM in the context of KWS. Since spectral flux reflects the degree of change between two adjacent frames, a fixed threshold method is adopted for its binarization. The SF threshold is set to 1024 in this implementation. The SF scratch pad (SPad) stores the Boolean value for 64 frames and sends them to the downstream feature bank. Since MFSC represents the energy of the current frame, and microphones have different gains, the fixed threshold method is impossible to meet practical needs. Previous TM works typically employ the quantile binning method for binarization, yet it introduces significant quantization errors since audio data is highly imbalanced. Therefore, a dynamic average thresholding circuit is proposed to realize streaming threshold updates. To eliminate the division of the average calculation, the batch size is set to 64, so that shifting can be used to approximate the division operation.

The threshold update process is executed in two cycles. In the first cycle, the original threshold is read from the threshold bank, and the new MFSC value is stored in the register. Simultaneously, the old MFSC value is read from the MFSC SPad according to the location where the new MFSC value is to be written. In the next cycle, the new threshold is obtained by adding the new MFSC value to the original threshold and subtracting the old MFSC value. For each inference, all data

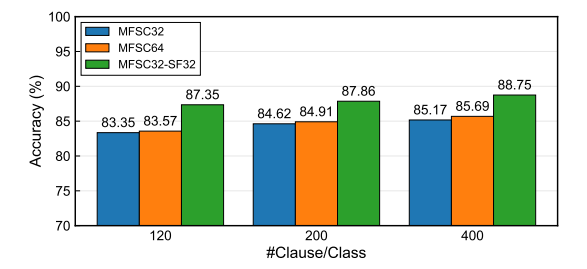


Fig. 7. Measured the accuracy of the CTM under different pre-processing algorithms and model scales. The 120-Clause CTM with MFSC32-SF32 is the selected model in this work.

stored in the MFSC SPad is read out for binarization. To improve parallelism, the MFSC SPad is divided into eight banks, allowing eight values to be read simultaneously. This binarization method allows for all memories to be mapped to single-port Static Random-Access Memory (SRAM).

We evaluate MFSC and MFSC-SF with varying coefficient sizes for feature extraction and train CTM models at different scales. Fig. 7 shows that the MFSC-SF algorithm effectively improves accuracy across different-sized CTM models. For instance, the 120-Clause CTM obtains a 4% accuracy gain when using MFSC-SF. Since CTM currently only supports single-layer models, the increase in the input feature dimension does not significantly affect the model size. However, the benefits of introducing the MFSC-SF algorithm allow the model to be scaled down to a smaller size without compromising accuracy.

C. OG-BCSR Algorithm

1) Overview: In this work, we choose a 64×7 convolution kernel. The selection of the convolution kernel size will be introduced in Section III-D. Since the convolution kernel of CTM contains positional TAs, we concatenate them into the matrix. To account for both positive and negative literals, the resulting TA action matrix has dimensions of 64×16 . For the 120-Clause CTM model, the size of the TA action

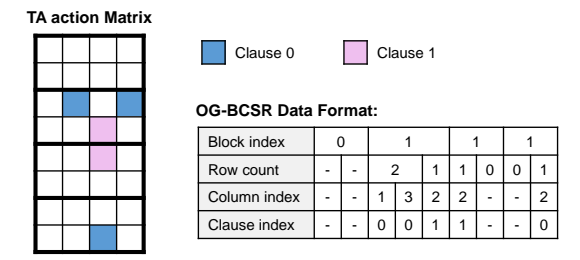


Fig. 8. Example of compressing the TA action matrix using OG-BCSR. The block index is used to skip storage of empty blocks, e.g., the first block is empty. The row count indicates the number of included TAs in each row. The column index indicates their column addresses.

matrix is 180 KB. To achieve efficient compression, we introduce an Optimized Grouped Block-Compressed Sparse Row algorithm, which maximizes the compression rate under given constraints. This algorithm is proposed based on the following observation: in highly sparse matrices, empty rows can diminish the compression efficiency of the standard Compressed Sparse Row (CSR) algorithm. We improve the compression rate through two methods: block compression and grouped compression. The purpose of block compression is to skip the unnecessary list storage using a block index list. The block index indicates whether there is an included TA in the block, and two rows are treated as one block in this work. The purpose of grouped compression is to reduce the sparsity rate of the matrix. Therefore, an additional clause index list is added to the list to indicate which clause the included TA comes from.

Fig. 8 shows an example of OG-BCSR compression. If the block is empty, storage of the subsequent list is skipped. Unlike the original CSR algorithm [30], we use direct row index storage instead of pointer storage. This is because the included TA only needs to be accessed sequentially and does not need to perform multiplications with other matrices. The use of direct storage can reduce the overhead of the decompression circuit.

2) Graph-Based Grouping: In the OG-BCSR algorithm, the grouping strategy directly influences the compression outcome. We observe that this problem can be transformed into a maximum weight matching problem in graph theory to obtain the optimal grouping scheme. This is because in the OG-BCSR compression list, the length of the block index list is fixed, while the lengths of the column index list and clause index list are determined by the number of included TAs. These lists cannot be optimized. Therefore, the optimal compression is achieved when the length of the row count list is minimized. Fortunately, the length of the row count list is positively correlated with the number of non-empty blocks, which can be known in advance before compression.

An example of converting matrix grouping into a graph is depicted in Fig. 9, where each TA action matrix is treated as a node (left), and nodes are connected pairwise to form a general graph (right). We define two constraints: if merging two matrices would result in overlapping non-zero elements or exceed the maximum allowable row count, they are considered to have no connecting edge, such as node 0 and node 2. The

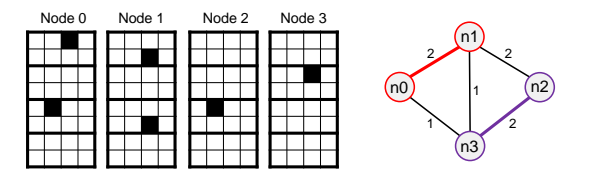


Fig. 9. Construction process from the TA action matrix to the graph. The weight of edges is the number of empty blocks after merging. In the example, n0-n1 and n2-n3 form the optimal matching.

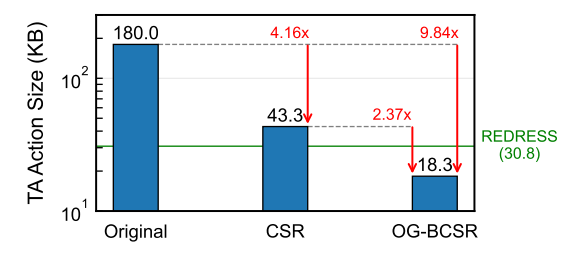


Fig. 10. Compression results of CSR and OG-BCSR algorithms.

optimization goal is to find a matching between nodes such that the total weight of the connecting edges between each pair of nodes is maximized, i.e., the scheme with the maximum number of empty blocks after merging is obtained. This maximum weight matching problem is solved using the Blossom algorithm [31], which efficiently identifies augmenting paths in general graphs.

We restrict the number of included TAs per row after merging to no more than 7. Due to the low similarity and high sparsity of the matrix, this constraint is only not satisfied in a few cases, which does not affect the optimal solution. Therefore, the row count list can be represented by 3 bits to reduce storage overhead. In this work, the total number of included TAs in the 120-Clause CTM model is 15.6k. After constructing the general graph, the maximum weight matching algorithm is applied to obtain the optimal grouping. The result is shown in Fig. 10, where the proposed OG-BCSR algorithm can further reduce the model size by $2.37 \times$ compared to CSR. Since the SoTA compression work, REDRESS [13], focuses on a 6-keyword task, we linearly scale its memory requirements to align with our task. The result demonstrates that our algorithm achieves a lower memory footprint.

D. Algorithm-Hardware Co-design

In this work, the algorithm-hardware co-design primarily consists of three parts: the spectral convolution operation, a state-driven architecture, and a two-stage scheduling optimization algorithm.

1) Spectral Convolution Operation: In CNNs, small convolution kernels are commonly used in multi-layer networks to accomplish specific recognition tasks. However, the current CTM remains a single-layer model, and related research [12] indicates that one Boolean value per coefficient is sufficient to represent most information. The use of small kernels will prevent the CTM model from having enough attention to recognize global spectral features. Therefore, the spectral convolution kernel is proposed to enhance feature extraction

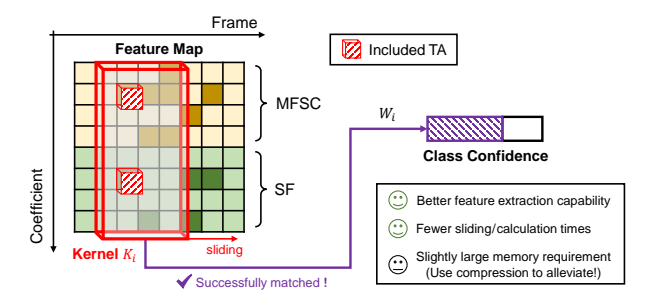


Fig. 11. The spectral convolution kernel covers the entire spectral coefficient dimension to achieve efficient feature matching. Two smiling faces denote the advantages of the spectral convolution kernel in terms of performance and power, while a neutral face represents an acceptable area trade-off. W_i refers to the weight of the convolution kernel K_i .

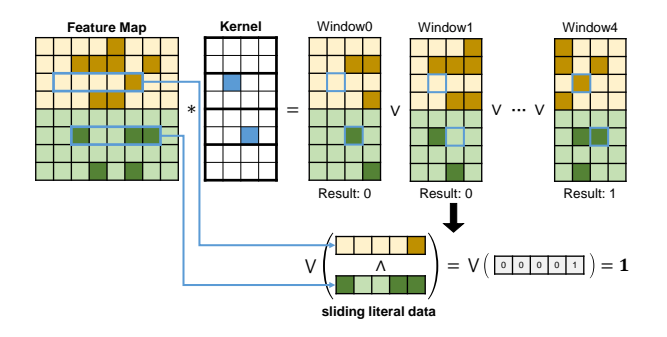


Fig. 12. The computation process of the CTM and the state-driven strategy. The sliding literal data is obtained according to the position of included TAs, and it is directly computed to equivalently achieve the convolution result.

capabilities. The red box in Fig. 11 depicts the spectral convolution kernel. The upper part of the feature map represents MFSC, while the lower part represents SF. Since MFSC and SF are temporally aligned, the convolution kernel can learn spectral representations on specific time slices. For instance, if the convolution kernel matches a specific window feature during the sliding process, the corresponding clause is satisfied, and its weight is output. This behavior matches the definition of the CTM model introduced in Section II-A, thus effectively achieving keyword feature recognition while ensuring interpretability.

2) State-Driven Architecture: As mentioned in Section II-B, in the data-driven architecture, the systolic array brings efficient data reuse and high parallelism, while it lacks flexibility in processing sparse data. In the event-driven architecture, the event-driven strategy can fully utilize the sparsity of input activations, while its parallelism is limited by the unpredictability of spiking events. Benefiting from the sparse determinism and high sparsity of the CTM, we propose a state-driven architecture that addresses the inherent limitations of the above two architectures.

Fig. 12 describes the convolution process and the state-driven strategy. The convolution kernel slides across the feature map to detect specific patterns. The result of the window is obtained by performing logical operations between the feature map and the kernel. In CTMs, the excluded TA represents "don't care", so we only need to focus on the feature map data corresponding to the included TA positions, i.e., the blue square in the window. When all the feature map

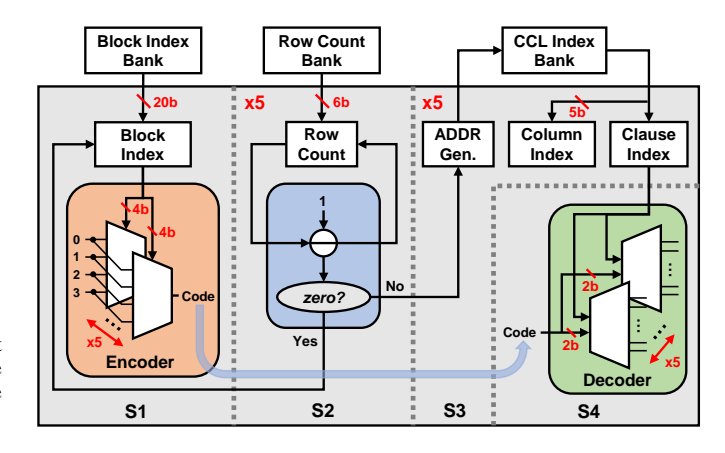


Fig. 13. The pipeline architecture of the OG-BCSR decompression circuit includes four stages: block index decompression (S1), row count decompression (S2), column index and clause index decompression (S3), and PE computation (S4). The 'x5' notation denotes five parallel hardware units.

data corresponding to the positions of blue squares are 1, it indicates that the window has a specific pattern. As long as the specific pattern is identified in any one window, the clause is satisfied. We found that for each included TA, the required data is the feature data covered by it during the sliding process. Therefore, the sliding process is unrolled to obtain our state-driven strategy.

Firstly, the row data of the feature map is read based on the row index of the included TA. Secondly, the actual covered data in the row data is selected based on the column index of the included TA. The data covered during sliding window operations is called sliding literal data. The length of sliding literal data is equal to the number of windows. Thirdly, logical AND operations are performed on the sliding literal data of each included TA to obtain the result for each sliding window. This step is performed in the PE array, so each PE only contains one AND gate. Finally, as long as the result of one sliding window is 1, the clause is satisfied. Thanks to the OG-BCSR algorithm, the index of included TAs can be obtained through decompression. When the included TAs are decompressed sequentially, the hardware architecture for a CTM with N windows is equivalent to an N×1 PE array.

To achieve horizontal reuse of input features, we employ a priority encoding scheme for decompression, rather than simply duplicating the hardware for parallel matrix decompression. This decision is motivated by two concerns: hardware overhead and utilization. Firstly, the behavior of the state-driven strategy unrolls all of the sliding window leads to the generation of multiplexers, which means that simply duplicating the hardware would introduce substantial hardware overhead. Secondly, to avoid access conflicts in the input feature bank, the matrix decompression process is performed synchronously: the next block begins processing only after finishing the decompression of all included TAs in the current block. Due to the high sparsity of the TA action matrix, synchronous decompression of multiple matrices results in low PE utilization. For instance, if only 6 out of 20 matrices contain included TAs in the current block, the utilization of the decompression logic and PEs falls below 30%.

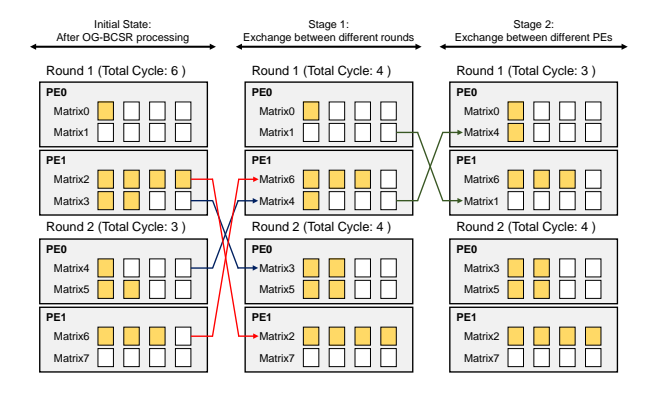


Fig. 14. Example of a two-stage scheduling optimization strategy.

Fig. 13 illustrates the pipeline architecture of the encoding and decompression circuit. In stage S1, the block indices of 20 TA action matrices are loaded into registers. The priority encoder groups every four matrices to generate five 2-bit "Code" signals, which are then allocated to the subsequent five parallel stages for control. In stage S2, to increase the memory bandwidth, the row count values of two rows are fetched into registers simultaneously. This value is then decremented each cycle to decompress included TAs sequentially. Stage S3 is activated whenever the row count value is non-zero, reading out the corresponding column and clause indices. Once the row count value reaches zero, the block index is updated to proceed to the following matrix. In stage S4, the partial logic AND (Pand) result is updated according to the "Code" signal and clause index. By applying the priority encoding method, 20 matrices are time-shared and allocated across five parallel decompression logic units and PE columns, effectively alleviating resource idleness.

3) Two-Stage Scheduling Optimization: The sparsity of TM models is unstructured, which presents a key hardware challenge in achieving load balancing under high parallelism. For event-driven architectures, due to the unpredictability of spiking events, additional load-balancing hardware is necessary, such as special dispatchers and rotating FIFOs. However, these load-balancing components are undesirable for the slight edge KWS hardware because they add extra cache and logic complexity. Due to the deterministic sparsity of TMs, the activity of the hardware can be simulated in software, representing the possibility of offline load balancing.

The purpose of load balancing is to improve hardware utilization and reduce computation cycles. We utilize the simulated annealing algorithm to achieve optimization, with the goal of minimizing the total cycles. Due to the enormous search space, the optimization process is divided into two stages to reduce the total cycles gradually. For the 120-clause CTM model, the 60 TA matrices per class are distributed in 5 PE columns over 3 rounds. In the first stage, matrices are randomly exchanged between different rounds to mitigate interround imbalance. In the second stage, matrices are exchanged between PEs within the same round to alleviate intra-round load variance.

Fig. 14 depicts a simplified example of the two-stage scheduling optimization strategy. In Stage 1, the imbalance

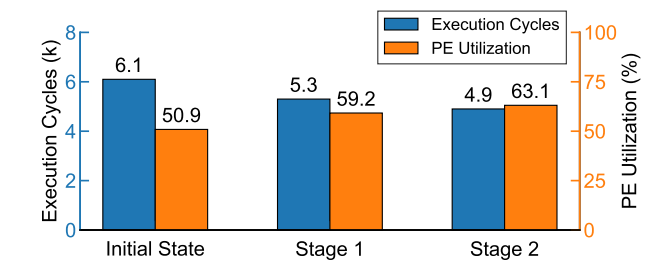


Fig. 15. Comparisons of the execution cycle and PE utilization in each optimization stage.

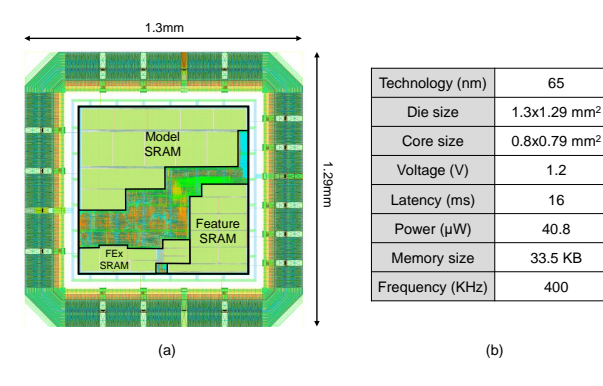


Fig. 16. (a) The layout of TsetlinKWS (exported from Cadence Virtuoso). (b) The performance metrics of TsetlinKWS.

between different rounds is alleviated after swapping. In Stage 2, the PEs within each round are further fine-tuned. Through this two-stage optimization, the idle period of PE0 in round 1 is decreased from 5 to 1, and the total computation period is shortened accordingly. We evaluate the two-stage scheduling optimization algorithm on the 120-clause CTM model. Fig. 15 shows the comparison of the execution cycles and PE utilization obtained by software simulations at each optimization stage. After two rounds of optimization, the PE utilization is increased to 63.1%, and a total of 1.2k cycles are saved, enabling the system to operate at a clock frequency of 400 KHz.

IV. IMPLEMENTATION AND MEASUREMENT RESULTS

A. Experimental Setup and Performance Measurement

In this work, the model parameters of TsetlinKWS are all stored on-chip by the SPI interface during initialization. The model is trained using the Google Speech Commands Dataset (GSCD) [32], which contains 35 keywords. Among them, ten command keywords are trained as primary keywords, including "Yes", "No", "Up", "Down", "Left", "Right", "On", "Off", "Stop", and "Go". Additionally, there are two categories: "Silence" (obtained from the background noise file) and "Unknown" (comprising the remaining 25 keywords), which are also included. During training, we only randomly add 20-40 dB of minor white noise [33] into the keyword audio, since the single-layer logic-based CTM model cannot handle high background noise effectively. Additionally, data augmentation is applied by randomly altering the audio pitch. The training, validation, and test sets contain 74922, 4490, and 4870 audio examples, respectively. The software code of

TABLE I COMPARISON OF SOTA KWS WORKS

	Batch-based Accelerator			Frame-based Accelerator	
	This work	TCASI'20 [6]	TCAD'20 [7]	JSSC'20 [11]	TCASAI'24 [10]
Technology	65 nm	22 nm	22 nm	65 nm	65 nm
Voltage (V)	0.7	0.6	0.8	0.6	0.6/0.65
Core Area (mm ²)	0.63	0.219	0.2	2.56	0.78
N. Core Area ^a (mm ²)	0.63	1.752	1.6	2.56	0.78
Sample Rate	16 KHz	16 KHz	16 KHz	16 KHz	8 KHz
System Frequency	400 KHz	250 KHz	250 KHz	250 KHz \sim 8 MHz	125 KHz
Power	16.58 μW	10.8 μW	8.15 μW	16.11 μW	$5.22 \ \mu W \ (\Delta TH = 0.2)$
Inference Core Power (Logic + SRAM)	11.94 µW (3.17 µW + 8.77 µW)	7.2 μW	8.15 μW (5.4 μW + 2.75 μW)	6.01 μW	3.91 µW (2.97 µW + 0.94 µW)
N. Inf. Core Power (Logic + SRAM) ^a	11.94 μW (<u>3.17</u> μW + 8.77 μW)	57.6 μW	65.2 μW (43.2 μW + 22 μW)	6.01 μW	3.91 µW (2.97 µW + 0.94 µW)
Latency (ms)	16	16	100	16	$6.9 \ (\Delta TH = 0.2)$
N. Inf. Core Energy ^a	191 nJ	921 nJ	6520 nJ	96 nJ	27 nJ (Δ TH = 0.2)
Model	CTM	BWN	TC-ResNet	LSTM	ΔGRU
Model Size	19.9 KB	4.4 KB	49.5 KB	10.1 KB ^b	14.8 KB
On-chip Memory	33.5 KB	10.7 KB	74.1 KB	96 KB	25.7 KB
Dataset	GSCD (12)	GSCD (12)	GSCD (12)	GSCD (12)	GSCD (12)
#Operations/Inference	907k AND	3m 16b Approx. ADD	1.27m 8*8b MUL + 1.27m 20b ADD	20k 8*8b MUL + 20k 32b ADD ^b	15k 8*12b MUL + 15k 12b ADD
#Norm_Ops./Inf.c	907k	120m	533m	9.8m ^b	9.3m (max)
Accuracy	87.35% @clean	87.9% @clean 84.4% @10dB 80.8% @5dB	93.09% @clean 90.49% @20dB	90.87% @clean	89.5% @clean

^a "N." denotes that the core area, inference core power, and energy are normalized to 65 nm.

^c Normalize the number of KWS operations per inference to 2-input AND gate operations.

the MFSC-SF pre-processing is designed to ensure numerical consistency with its hardware counterpart. For the 120-Clause CTM model, the hyperparameters T and s are set to 300 and 8.0, respectively. The model is trained with 400 epochs.

The proposed design is implemented and evaluated under TSMC 65 nm LP CMOS technology. Clock gating and operand isolation techniques are applied to further reduce power consumption. Fig. 16(a) and Fig. 16(b) show the layout and measurement results of TsetlinKWS, respectively. Due to the lack of a low-voltage library, power measurements are conducted at 25 °C and 1.2 V, excluding IO Pad power. The core power at 1.2 V is 40.8 µW. The die area and core area are 1.67 mm² and 0.63 mm², respectively. Onchip memory includes feature extraction SRAM (1.53 KB), model SRAM (27.25 KB), and feature SRAM (4.75 KB). The proposed system performs feature extraction and inference at a frequency of 400 KHz. Additionally, an 8.192 MHz I2S master clock is divided to generate a 1.024 MHz bit clock and a 16 KHz frame clock, which controls the external I2S digital microphone module for audio data acquisition.

For KWS applications, the operating voltage can generally be scaled down below 0.7 V without timing violations, as the low operating frequency provides sufficient timing margin. To facilitate fair comparison with other works, we scale dynamic

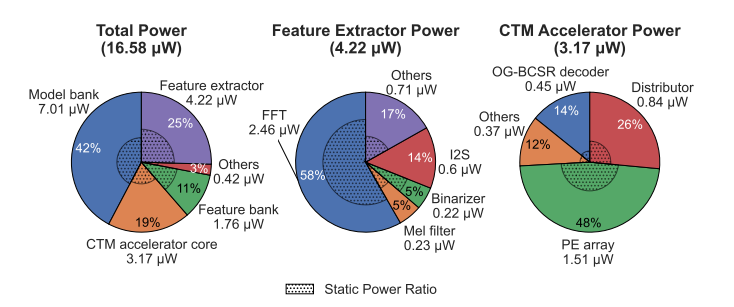


Fig. 17. Power breakdown of TsetlinKWS, feature extractor, and CTM accelerator at 0.7 V.

power by the square of the voltage ratio and static power by the voltage ratio. This is a conservative estimate for leakage power, as it does not account for the additional reduction in leakage current at lower voltages. The core voltage is scaled from 1.2 V to 0.7 V for this analysis.

Fig. 17 shows the power breakdown at 0.7 V. After voltage scaling, the core power is decreased from 40.8 μ W to 16.58 μ W. The 27.25 KB SRAM used for storing the CTM model accounts for 42% of the total power. The power of the feature extractor and feature bank is 4.22 μ W and 1.76 μ W, respectively. Within the feature extractor, the FFT module dominates the power consumption. This is because

b Assuming the structure of the LSTM model is: input(13)-hidden(64)-output(12). The model parameters are 4 bits, and are restored to 8 bits during calculation.

other modules employ various low-power techniques to reduce computational complexity, whereas the FFT scheme adopted in this work is not the optimal choice for real-valued audio signal processing. The optimization of the FFT is not included in this work. For the CTM accelerator, the majority of the power is consumed by the PE array, including its internal 2320 Pand registers, as expected. This overhead is a direct result of our design goal to achieve sparse acceleration with minimal control overhead. Both the FFT and PE array exhibit relatively high leakage power ratios compared to other modules. As the leakage power estimation is conservative, actual power consumption is expected to be even lower.

B. Comparison With SoTA Works

Table I compares the state-of-the-art KWS accelerator with our proposed design. All KWS chips are categorized into two types: batch-based accelerators and frame-based accelerators.

Among batch-based approaches, Liu et al. [6] proposed a Binary Weight Network (BWN) accelerator to eliminate multiplication operations, achieving an inference core power of 7.2 µW in 22 nm technology. Although approximate addition is employed, 120 million equivalent AND operations per inference are required. Bernardo et al. [7] used a shallow TC-ResNet to achieve 93.09% accuracy, yet it demands 1.27 million Multiply-Accumulate (MAC) operations per inference, resulting in 100 ms latency even with early exiting.

On the other hand, frame-based accelerators achieve higher efficiency by processing features sequentially. Giraldo et al. [11] employed a single-layer long short-term memory (LSTM) network that consumes 6.01 μ W and requires only 20 kilo MAC operations per inference. Chen et al. [10] designed a custom memory architecture to reduce SRAM power by 6.6×, achieving an inference core power of 3.91 μ W.

Compared to other batch-based accelerators, our design achieves at least 4.8× reduction in inference core power and a significantly smaller core area. Notably, to the best of our knowledge, TsetlinKWS is the first batch-based KWS accelerator, which achieves a competitive logic inference core power compared to other frame-based KWS accelerators. Furthermore, TsetlinKWS requires the fewest gate-level operations per inference, even fewer than frame-based accelerators, which process only a single frame per inference.

C. Discussion

According to experimental results, the Convolutional Tsetlin Machine, as an emerging AI algorithm, demonstrates remarkable potential for keyword spotting tasks. In this paper, we construct a complete KWS hardware system and compare it with the SoTA neural network accelerators. On the basis of rigorously demonstrating its power consumption advantage, we provide new insights for the hardware architecture design of CTMs. The following is a further explanation and analysis of the implementation outcomes:

1) Flexible category scaling: The CTM model used in this work does not share parameters across categories. Therefore, when the required keyword categories are reduced, the model size will be linearly reduced, which can alleviate the current

large memory overhead and computational latency. For example, when only two keywords are needed, the number of logical operations per frame will be reduced to 150k.

- 2) Memory optimization potential: Due to the limited feature extraction capability of the single-layer CTM model, the CTM model is larger in size than NN-based models. For the power consumption of AI accelerators, besides computational logic, memory access is equally important. Therefore, techniques such as memory bank division, setting up nearend caches, and customizing dedicated memory blocks can effectively further reduce system power consumption.
- 3) Robust feature extraction algorithm: In our experiments, we found that due to the high sensitivity of logic-based models to background noise, the KWS system proposed in this work is only suitable for near-microphone scenarios. Feature extractors designed based on bio-acoustic features have been shown to outperform MFCC in robustness [34]. Combining a more robust feature extraction algorithm with the CTM is an effective choice to mitigate this limitation.
- 4) Advantages and challenges: Frame-based accelerators currently remain more energy-efficient for KWS inference. However, our results indicate that CTMs can achieve competitive power efficiency on audio tasks compared with frame-based accelerators. The simple learning method of CTMs further indicates that it is a promising solution for edge speech applications, which demand high privacy and adaptability. An important issue at present is that if the accuracy requirement exceeds 90%, a larger CTM model size is required, which means that model size and memory access deserve more attention in future CTM research.

V. CONCLUSION

This paper proposes a Convolutional Tsetlin Machine-based KWS chip through algorithm-hardware co-design, featuring an MFSC-SF feature extractor, the spectral convolution operation, and a state-driven architecture with fully sparse utilization and efficient data reuse. By compressing and scheduling the determined sparse model parameters, the optimal model size and execution cycle are obtained. The proposed TsetlinKWS chip achieves a power of $16.58~\mu W$ and a core area of $0.63~mm^2$ at 65~nm. Our design enables deterministic sequential access to all model memories, providing further memory optimization space. The additional introduction of spectral flux features effectively improves accuracy through low hardware overhead, enabling TsetlinKWS to achieve a classification accuracy of 87.35% on the 12-keyword spotting task.

ACKNOWLEDGMENTS

The authors would like to acknowledge the Novel IC Exploration Facility at the Hong Kong University of Science and Technology (Guangzhou) for providing experimental support, and Ms. Zheng Yujin of Newcastle University for help with backend script writing. This work was supported by the Engineering and Physical Sciences Research Council (EPSRC), UK, under the projects *MultiTasking and Continual Learning for Audio Sensing Tasks on Resource-Constrained Platforms* (EP/X01200X/1).

REFERENCES

- [1] T. Rahman, G. Mao, S. Maheshwari, R. Shafik, and A. Yakovlev, "Matador: Automated system-on-chip tsetlin machine design generation for edge applications," in 2024 Design, Automation & Test in Europe Conference & Exhibition (DATE). IEEE, 2024, pp. 1–6.
- [2] S. A. Tunheim, L. Jiao, R. Shafik, A. Yakovlev, and O.-C. Granmo, "Tsetlin machine-based image classification fpga accelerator with ondevice training," *IEEE Transactions on Circuits and Systems I: Regular Papers*, 2024.
- [3] G. Mao, T. Rahman, S. Maheshwari, B. Pattison, Z. Shao, R. Shafik, and A. Yakovlev, "Dynamic tsetlin machine accelerators for on-chip training using fpgas," *IEEE Transactions on Circuits and Systems I: Regular Papers*, 2025.
- [4] B. Liu, N. Xie, R. Zhang, H. Yang, Z. Wang, D. Fan, Z. Wang, W. Liu, and H. Cai, "A 3.8-\(\mu\)w 10-keyword noise-robust keyword spotting processor using symmetric compressed ternary-weight neural networks," *IEEE Open Journal of the Solid-State Circuits Society*, vol. 3, pp. 185–196, 2023.
- [5] T.-J. Lin, Y.-H. Ting, M.-Z. Hsu, K.-H. Lin, C.-M. Huang, F.-C. Tsai, S.-S. Sheu, S.-C. Chang, C. Yeh, and J.-S. Wang, "A 16 nm 140 tops/w 5 μj/inference keyword spotting engine based on 1d-bcnn," *IEEE Transactions on Circuits and Systems II: Express Briefs*, vol. 70, no. 12, pp. 4564–4568, 2023.
- [6] B. Liu, H. Cai, Z. Wang, Y. Sun, Z. Shen, W. Zhu, Y. Li, Y. Gong, W. Ge, J. Yang et al., "A 22nm, 10.8 μw/15.1 μw dual computing modes high power-performance-area efficiency domained background noise aware keyword-spotting processor," *IEEE Transactions on Circuits and Systems I: Regular Papers*, vol. 67, no. 12, pp. 4733–4746, 2020.
- [7] P. P. Bernardo, C. Gerum, A. Frischknecht, K. Lübeck, and O. Bringmann, "Ultratrail: A configurable ultralow-power tc-resnet ai accelerator for efficient keyword spotting," *IEEE Transactions on Computer-Aided Design of Integrated Circuits and Systems*, vol. 39, no. 11, pp. 4240–4251, 2020.
- [8] Y. S. Chong, W. L. Goh, V. P. Nambiar, and A.-T. Do, "A 2.5 μw kws engine with pruned lstm and embedded mfcc for iot applications," *IEEE Transactions on Circuits and Systems II: Express Briefs*, vol. 69, no. 3, pp. 1662–1666, 2021.
- [9] C. Frenkel and G. Indiveri, "Reckon: A 28nm sub-mm2 task-agnostic spiking recurrent neural network processor enabling on-chip learning over second-long timescales," in 2022 IEEE International Solid-State Circuits Conference (ISSCC), vol. 65. IEEE, 2022, pp. 1–3.
- [10] Q. Chen, K. Kim, C. Gao, S. Zhou, T. Jang, T. Delbruck, and S.-C. Liu, "Deltakws: A 65nm 36nj/decision bio-inspired temporal-sparsity-aware digital keyword spotting ic with 0.6 v near-threshold sram," *IEEE Transactions on Circuits and Systems for Artificial Intelligence*, 2024.
- [11] J. S. P. Giraldo, S. Lauwereins, K. Badami, and M. Verhelst, "Vocell: A 65-nm speech-triggered wake-up soc for 10-µw keyword spotting and speaker verification," *IEEE Journal of Solid-State Circuits*, vol. 55, no. 4, pp. 868–878, 2020.
- [12] J. Lei, T. Rahman, R. Shafik, A. Wheeldon, A. Yakovlev, O.-C. Granmo, F. Kawsar, and A. Mathur, "Low-power audio keyword spotting using tsetlin machines," *Journal of Low Power Electronics and Applications*, vol. 11, no. 2, p. 18, 2021.
- [13] S. Maheshwari, T. Rahman, R. Shafik, A. Yakovlev, A. Rafiev, L. Jiao, and O.-C. Granmo, "Redress: Generating compressed models for edge inference using tsetlin machines," *IEEE Transactions on Pattern Analysis and Machine Intelligence*, vol. 45, no. 9, pp. 11152–11168, 2023.
- [14] S. A. Tunheim, Y. Zheng, L. Jiao, R. Shafik, A. Yakovlev, and O.-C. Granmo, "An all-digital 65-nm tsetlin machine image classification accelerator with 8.6 nj per mnist frame at 60.3 k frames per second," arXiv e-prints, pp. arXiv-2501, 2025.
- [15] K. D. Abeyrathna, O.-C. Granmo, and M. Goodwin, "Extending the tsetlin machine with integer-weighted clauses for increased interpretability," *IEEE Access*, vol. 9, pp. 8233–8248, 2021.
- [16] O.-C. Granmo, S. Glimsdal, L. Jiao, M. Goodwin, C. W. Omlin, and G. T. Berge, "The convolutional tsetlin machine," arXiv preprint arXiv:1905.09688, 2019.
- [17] A. Bakar, T. Rahman, A. Montanari, J. Lei, R. Shafik, and F. Kawsar, "Logic-based intelligence for batteryless sensors," in *Proceedings of the 23rd Annual International Workshop on Mobile Computing Systems and Applications*, 2022, pp. 22–28.
- [18] S. Yin, P. Ouyang, S. Tang, F. Tu, X. Li, L. Liu, and S. Wei, "A 1.06-to-5.09 tops/w reconfigurable hybrid-neural-network processor for deep learning applications," in 2017 Symposium on VLSI Circuits. IEEE, 2017, pp. C26–C27.

- [19] S. Han, J. Pool, J. Tran, and W. Dally, "Learning both weights and connections for efficient neural network," Advances in neural information processing systems, vol. 28, 2015.
- [20] S. Zhang, Z. Du, L. Zhang, H. Lan, S. Liu, L. Li, Q. Guo, T. Chen, and Y. Chen, "Cambricon-x: An accelerator for sparse neural networks," in 2016 49th Annual IEEE/ACM International Symposium on Microarchitecture (MICRO). IEEE, 2016, pp. 1–12.
- [21] A. Parashar, M. Rhu, A. Mukkara, A. Puglielli, R. Venkatesan, B. Khailany, J. Emer, S. W. Keckler, and W. J. Dally, "Scnn: An accelerator for compressed-sparse convolutional neural networks," ACM SIGARCH computer architecture news, vol. 45, no. 2, pp. 27–40, 2017.
- [22] C. Deng, Y. Sui, S. Liao, X. Qian, and B. Yuan, "Gospa: An energy-efficient high-performance globally optimized sparse convolutional neural network accelerator," in 2021 ACM/IEEE 48th Annual International Symposium on Computer Architecture (ISCA). IEEE, 2021, pp. 1110–1123
- [23] S. Narayanan, K. Taht, R. Balasubramonian, E. Giacomin, and P.-E. Gaillardon, "Spinalflow: An architecture and dataflow tailored for spiking neural networks," in 2020 ACM/IEEE 47th Annual International Symposium on Computer Architecture (ISCA). IEEE, 2020, pp. 349– 362.
- [24] J. Sommer, M. A. Özkan, O. Keszocze, and J. Teich, "Efficient hardware acceleration of sparsely active convolutional spiking neural networks," *IEEE Transactions on Computer-Aided Design of Integrated Circuits* and Systems, vol. 41, no. 11, pp. 3767–3778, 2022.
- [25] P. Plagwitz, F. Hannig, J. Teich, and O. Keszocze, "To spike or not to spike? a quantitative comparison of snn and cnn fpga implementations," arXiv preprint arXiv:2306.12742, 2023.
- [26] M. Blott, T. B. Preußer, N. J. Fraser, G. Gambardella, K. O'brien, Y. Umuroglu, M. Leeser, and K. Vissers, "Finn-r: An end-to-end deeplearning framework for fast exploration of quantized neural networks," ACM Transactions on Reconfigurable Technology and Systems (TRETS), vol. 11, no. 3, pp. 1–23, 2018.
- [27] Y. Jiao, Y. K. Li, C. H. Chan, Y. Li, and Z. Ai, "Thermometer code of log mel-frequency spectral coefficient for bnn-based keyword spotting system," in 2022 IEEE Asia Pacific Conference on Circuits and Systems (APCCAS). IEEE, 2022, pp. 414–418.
- [28] J. Lei, A. Wheeldon, R. Shafik, A. Yakovlev, and O.-C. Granmo, "From arithmetic to logic based ai: A comparative analysis of neural networks and tsetlin machine," in 2020 27th IEEE international conference on electronics, circuits and systems (ICECS). IEEE, 2020, pp. 1–4.
- [29] W. Han, C.-F. Chan, C.-S. Choy, and K.-P. Pun, "An efficient mfcc extraction method in speech recognition," in 2006 IEEE International Symposium on Circuits and Systems (ISCAS). IEEE, 2006, pp. 4–pp.
- [30] S. Filippone, V. Cardellini, D. Barbieri, and A. Fanfarillo, "Sparse matrix-vector multiplication on gpgpus," ACM Transactions on Mathematical Software (TOMS), vol. 43, no. 4, pp. 1–49, 2017.
- [31] Z. Galil, "Efficient algorithms for finding maximum matching in graphs," ACM Computing Surveys (CSUR), vol. 18, no. 1, pp. 23–38, 1986.
- [32] P. Warden, "Speech commands: A dataset for limited-vocabulary speech recognition," arXiv preprint arXiv:1804.03209, 2018.
- [33] A. Varga and H. J. Steeneken, "Assessment for automatic speech recognition: Ii. noisex-92: A database and an experiment to study the effect of additive noise on speech recognition systems," *Speech communication*, vol. 12, no. 3, pp. 247–251, 1993.
- [34] D. Wang, S. J. Kim, M. Yang, A. A. Lazar, and M. Seok, "9.9 a background-noise and process-variation-tolerant 109nw acoustic feature extractor based on spike-domain divisive-energy normalization for an always-on keyword spotting device," in 2021 IEEE International Solid-State Circuits Conference (ISSCC), vol. 64. IEEE, 2021, pp. 160–162.



Baizhou Lin received the B.Eng. degree in electronic and computer engineering from Shantou University, China, in 2022, and the M.Sc. degree in microelectronics systems design from the University of Southampton, UK, in 2024. His research interests include AI accelerators, FPGA, and algorithm-hardware co-design.



Yuetong Fang is currently a Ph.D candidate in Microelectronics Thrust, the Hong Kong University of Science and Technology (Guangzhou), China. Her research focuses on neuromorphic computing and hardware acceleration.



Renjing Xu is an Assistant Professor in the Microelectronics Thrust of the Function Hub and the Robotics and Autonomous Systems Thrust of the System Hub at the Hong Kong University of Science and Technology (Guangzhou). He received a B.Eng in systems engineering from the Australian National University in 2015 and a Ph.D from Harvard University in 2021. From 2015 to 2016, he was a Visiting Scholar with the Photonics Laboratory, University of Wisconsin-Madison, Madison, USA. His research interests include human-centered com-

puting and hardware-efficient computing.



Rishad Shafik (Senior Member) is a Professor of Microelectronic Systems within the School of Engineering, Newcastle University, UK. Professor Shafik received his PhD, and MSc (with distinction) degrees from Southampton in 2010, and 2005; and BSc (with distinction) from the IUT, Bangladesh in 2001. He is one of the editors of the Springer USA book "Energy-efficient Fault-tolerant Systems". He is also author/co-author of 200+ IEEE/ACM peer-reviewed articles, with 4 best paper nominations and 3 best paper/poster awards. He recently chaired

multiple international conferences/symposiums, UKCAS2020, ISCAS2025, ISTM2022; guest edited special theme issues in Royal Society Philosophical Transactions A; he recently chaired IEEE SAS2025. His research interests include hardware/software co-design for machine learning systems.



Jagmohan Chauhan is an Assistant Professor in Computer Science at UCL. He received his PhD from the University of New South Wales. He has co-authored more than 50 research papers and has won three best paper awards. His research interests include machine learning systems, trustworthy machine learning, robotics, and designing and evaluating novel mobile systems and applications.